Journal of Molecular Catalysis A: Chemical 315 (2010) 213–220

Contents lists available at ScienceDirect

Journal of Molecular Catalysis A: Chemical

journal homepage: www.elsevier.com/locate/molcata

Microporous and mesoporous supports and their effect on the performance of supported metallocene catalysts

Fernando Silveira[a], Maria do Carmo Martins Alves[a], Fernanda C. Stedile[a], Sibele B. Pergher[b], João Henrique Zimnoch dos Santos[a,*]

[a] Instituto de Química, UFRGS, Av. Bento Gonçalves, 9500 – Porto Alegre, 91509-900, Brazil
[b] Departamento de Química, Universidade Regional Integrada do Alto Uruguai e das Missões (URI) - Campus Erechim, CP 743, Erechim, 99700-000, Brazil

ARTICLE INFO

Article history:
Received 29 July 2009
Received in revised form
19 September 2009
Accepted 21 September 2009
Available online 1 October 2009

Keywords:
Supported metallocene
Polyethylene
Microporous supports
Mesoporous supports
EXAFS

ABSTRACT

A series of hybrid-supported catalysts was prepared by sequentially grafting Cp_2ZrCl_2 and $(n\text{BuCp})_2ZrCl_2$ (1:3 ratio) onto synthesized silica–zirconia xerogel, alumino-silicates, alumina, chrysotile and commercial MAO (methylaluminoxane)-modified silica. Supported catalysts were characterized by Rutherford backscattering spectrometry, atomic force microscopy, extended X-ray absorption fine structure spectroscopy, X-ray diffraction and nitrogen adsorption. The grafted metal content was between 0.21 and 1.00 wt.% Zr/SiO_2 or Zr/Al_2O_3. All of the systems were shown to be active in ethylene polymerization with methylaluminoxane as the cocatalyst. The catalyst activity and polymer molecular weight depended on the effects of the textural characteristics of the supports on the structure of the generated supported catalyst species. The highest activity in ethylene polymerization (ca. 6560 kgPE molZr^{-1} h^{-1}) was reached with the supported catalyst using commercial MAO-modified silica and also presented the lowest surface roughness. Correlation between EXAFS data and polymer characteristics was extracted: the production of polyethylenes with higher molecular weight was associated with the reduction in the interatomic Zr–O distance of the supported catalysts, which was shown to be dependent on the nature of the support.

1. Introduction

Metallocenes are compounds consisting of two cyclopentadienyl (Cp) anions bound to a metal center in a pentahapto (η^5) way, denoting the equivalent bonding of all five-carbon atoms. Supported metallocenes have been investigated in the last 20 years, although mostly exploring silica as their support [1,2]. Nevertheless, other types of supports have also been evaluated for the immobilization of metallocenes, aiming to increase catalyst activity or to exhibit different polymer properties. Some examples of different supports are zirconium phosphonates [3], magnesium chloride-based supports [4] and zeolites [5,6] just to mention a few.

Some studies have investigated the use of mesoporous materials and of ordered microporous silicates in the immobilization of metallocenes. MCM-41, SBA-15, and MCM-48 have been employed as supports for metallocenes [7,8], which includes the synthesis of syndiotatic [9] and isotatic [10] polypropylene or polyethylene nanofibers by extrusion through the mesopores of the supports [11,12]. SBA-15 was employed as a support for *in situ* zirconocene synthesis [13] and for the immobilization of Cp_2ZrCl_2 [14,15]. The chemical modification of SBA-15 with sulfonic acid prior to metallocene immobilization was used for the polymerization of ethylene [16]. Crystalline microporous zeolite such as MCM-22 has also been investigated. Chromium complexes were supported on MCM-22 for the ethylene polymerization by using MAO as cocatalyst [17]. Recently, nanosized ZSM-2 zeolite has been proposed as potential polymerization catalyst support [18].

The performance of an immobilized metallocene may be changed in comparison to its homogeneous counterpart by the electronic and steric effects of the support. Most of the supported metallocenes have exhibited lower catalytic activities in comparison to the homogenous ones. According to the literature, the reduction in the catalytic activity has been attributed to: (i) deactivation of the metallocene complexes during the grafting reaction, (ii) inaccessibility of the metallocene complexes to the cocatalyst (methylaluminoxane, MAO) and therefore hindering its activation; and (iii) restrictions of the monomer access to the active sites, thereby hindering the chain propagation [19]. Generally, the polymers produced with supported metallocenes have higher average molecular weights due to a reduction in the rate of the termination reactions [20]. Thus, the nature of the support seems to play a very relevant role in the performance of the supported metallocene.

In previous studies, we reported the effect of the microstructures of different silica-based supports on the structure of the grafted metallocenes [21] and textural properties of mesoporous materials on the activity and polymerization performance of the

* Corresponding author. Tel.: +55 51 3308 7238; fax: +55 51 3308 7304.
E-mail address: jhzds@iq.ufrgs.br (J.H.Z. dos Santos).

1381-1169/$ – see front matter © 2009 Elsevier B.V. All rights reserved.
doi:10.1016/j.molcata.2009.09.014

resulting supported metallocenes [22]. In the present study, as an extension of our previous works, we comparatively investigated the effect of the microstructures of different microporous and mesoporous supports on the structure of the resulting grafted metallocene species and on their performance in the polymerization of ethylene. Different microporous and mesoporous supports were employed that differed in their chemical nature (alumina, alumino-silicates, silica–zirconia, magnesium silicate support) or crystallographic arrangement (amorphous, crystalline and ordered materials). Thus, a series of supports, namely, SBA-15, ITQ-2, MCM-22, Al_2O_3, commercial MAO-modified silica, SiO_2-ZrO_2 (silica synthesized by the non-hydrolytic sol–gel method, employing $ZrCl_4$ as the Lewis acid catalyst), and natural chrysotile (silica nanofibers coated by a layer of brucite, $Mg(OH)_2$) was used. In addition, Cp_2ZrCl_2 and $(n\text{BuCp})_2ZrCl_2$ were sequentially grafted onto these supports in a 1:3 ratio in order to achieve a roughly equal amount of both catalysts on the surface [23]. The resulting catalysts were characterized by Rutherford backscattering spectrometry (RBS), atomic force microscopy (AFM), extended X-ray absorption structure (EXAFS) spectroscopy and nitrogen adsorption. The hybrid-supported catalysts were evaluated for ethylene polymerization with MAO as the cocatalyst. The polymers were characterized by gel permeation chromatography (GPC), differential scanning calorimetry (DSC), X-ray diffraction (XRD) spectroscopy and scanning electron microscopy (SEM).

2. Experimental

2.1. Materials

All of the chemicals were manipulated under an inert atmosphere using Schlenk techniques. Chrysotile was kindly provided by SAMA (Goiás, Brazil), SBA-15 was prepared at the Instituto de Tecnología Química de Valencia – ITQ-UPV (Spain), silica-MAO with 23 wt.% Al/SiO_2 (Witco) and alumina (INLAB, Brazil) were used without further purification. MCM-22 and ITQ-2 were prepared according to the literature [24,25]. Silica xerogel was prepared by the non-hydrolytic sol–gel process [26]. Furthermore, $(n\text{BuCp})_2ZrCl_2$ (Aldrich), Cp_2ZrCl_2 (Aldrich) and MAO (Witco, 10.0 wt.% toluene solution) were used without further purification. Pure grade toluene was deoxygenated and dried by standard techniques before use. Ethylene and argon (White Martins) were passed through a molecular sieve (13 Å) prior to use. Toluene was purified by refluxing with sodium, followed by distillation under nitrogen just before use.

2.2. Synthesis of the supported hybrid catalysts

All of the supports (MCM-22, ITQ-2, SBA-15, MAO-modified silica, alumina, silica–zirconia and chrysotile) were activated under vacuum ($P < 10^{-5}$ bar) for 16 h at 450 °C. In a typical experiment, a Cp_2ZrCl_2 toluene solution, corresponding to a 0.25 wt.% Zr/SiO_2, was added to ca. 1.0 g of the pre-activated support and stirred for 30 min at room temperature. Then, the solvent was removed under a vacuum through a fritted disk. A $(n\text{BuCp})_2ZrCl_2$ toluene solution, corresponding to a 0.75 wt.% Zr/SiO_2, was added, and the resulting slurry was stirred for more than 30 min at room temperature, and then filtered through a fritted disk. The resulting solids were washed with $10 \times 2.0\,cm^3$ of toluene and dried under vacuum for 4 h.

The same procedure was applied for all of the activated supports (MCM-22, ITQ-2, SBA-15, silica-MAO, alumina, silica–zirconia produced by the non-hydrolytic sol–gel route and natural chrysotile). The resulting supported catalyst systems were named M22, IT2, S15, SMAO, ALU, NHI and nCR after catalyst grafting.

2.3. Characterization of supported catalysts

2.3.1. Rutherford backscattering spectrometry (RBS)

Zirconium loadings in the catalysts were determined by RBS using He^+ beams of 2.0 MeV incident on homogeneous tablets of the compressed (12 MPa) powder of the catalyst systems. The method is based on the determination of the number and energy of the detected particles that are elastically scattered in the Coulombic field of the atomic nuclei in the target. In this study, the Zr/Si or Zr/Al atomic ratio was determined by the heights of the signals corresponding to each of the elements in the spectra and converted to wt.% Zr/SiO_2 or Al_2O_3. Precision was ca. 8%. For an introduction to the method and applications of this technique, the reader is referred elsewhere [27].

2.3.2. Nitrogen adsorption–desorption isotherms

Samples were previously degassed (10^{-2} mbar) at 120 °C (silica) or at 85 °C (supported catalysts) for 8 h. Adsorption–desorption nitrogen isotherms were measured at −196 °C in a Gemini 2375 (Micromeritics). Specific surface areas (S_{BET}) were determined by the Brunauer–Emmett–Teller equation ($P/P_0 = 0.05$–0.35). The mesopore size and distribution were calculated by the Barrett–Joyner–Halenda (BJH method) using the Halsey standards. The desorption branches were used.

2.3.3. Atomic force microscopy (AFM)

Images of supported catalyst surfaces were obtained using a Nanoscope IIIa® atomic force microscope, manufactured by Digital Instruments Co., using the contact mode technique with silicon nitride probes. The WS M 4.0 software from Nanotec Electronic S.L. [28] was used for the treatment of the images and the calculation of roughness (RMS). The samples were compressed in the form of agglomerates of roughly 16 mm^2 for the analysis.

2.3.4. Extended X-ray absorption fine structure (EXAFS)

The EXAFS measurements were performed around the Zr K edge ($E = 17{,}998$ eV) using the Si(220) channel-cut monochromator at the XAFS 1 beamline (LNLS, Campinas, Brazil). The spectra were collected in the fluorescence mode using one ionization chamber filled with argon and a Si(Li) detector. In order to perform the EXAFS experiments, the powder of the supported metallocenes was compacted into a pellet and covered with Kapton® tape. All of the manipulations were performed in a dry box to avoid any oxidation reactions. The EXAFS spectra were acquired from 17,900 to 18,900 eV with 3 eV steps. Several scans were averaged in order to improve the signal-to-noise ratio.

The IFEFFIT analysis package [29] and the Winxas program [30] were used for the EXAFS data analysis. The EXAFS signals between 1.0 and 10.0 $Å^{-1}$ were Fourier transformed with a k^1 weighting and a Bessel window. Structural parameters were obtained from least squares fitting in k and R space using theoretical phase shift and amplitude functions deduced from the FEFF7 code [29]. The input for the FEFF7 code was provided by the ATOMS program [31]. In the fitting procedure, the amplitude reduction factor (S_0^2) was close to 1.0 for all samples, and the threshold energies (E_0) for the Zr–C and Zr–O pair were −7.5 and −3.5 eV, respectively.

2.4. Polymerization reactions

Polymerizations were performed in toluene (0.15 L) in a 0.30-L Pyrex glass reactor connected to a constant temperature circulator equipped with mechanical stirring and inlets for argon and monomers. For each experiment, a mass of the catalyst system corresponding to 10^{-5} mol L^{-1} of Zr was suspended in 0.01 L of toluene and transferred into the reactor under argon. The polymerizations were performed at atmospheric pressure of ethylene at

Table 1
Grafted metal content, textural characteristics and catalyst activity in ethylene polymerization of the different supported systems.

Catalysts	Zr/SiO_2 (wt.%)	Specific surface area ($m^2\ g^{-1}$)	Zr density (Zr nm^{-2})	Pore diameter (Å)	Catalytic activity (kgPE $molZr^{-1}\ bar^{-1}\ h^{-1}$)
NHI	0.41[a]	18 ± 1	1.50	36	720
nCR	0.21	14 ± 0	0.98	39	400
SMAO[b]	1.00	99 ± 1	0.67	84	6560
ALU	0.90[c]	103 ± 1	0.60	42	853
S15	0.42	463 ± 0	0.06	50	3200
IT2	0.61	478 ± 0	0.08	14	1260
M22	0.51	313 ± 2	0.11	15	1467

[Zr] = 10^{-5} mol L^{-1}; [Al/Zr] = 1000; V = 0.15 L (toluene); P = 1 bar (ethylene); T = 60 °C; t = 30 min.
[a] $ZrCl_4$ was used as Lewis acid catalyst during the synthesis, resulting in 12.9 wt.% Zr/SiO_2 in the support. The Zr content reported on Table 1 corresponds from that resulting from the zirconocene immobilization.
[b] 23 wt.% Al/SiO_2.
[c] Supported on Al_2O_3, and therefore, Zr/Al_2O_3.

60 °C for 30 min at Al/Zr = 1000, using MAO as the cocatalyst. Acidified (HCl) ethanol was used to quench the processes; the reaction products were separated by filtration, washed with distilled water, and finally dried under reduced pressure at 60 °C.

2.5. Polyethylene characterization

The molar masses and molar mass distributions were investigated with a Waters CV plus 150C high-temperature GPC instrument, equipped with a viscosimetrical detector, and three Styragel HT-type columns (HT3, HT4 and HT6) with an exclusion limit of 1×10^7 for polystyrene. The solvent was 1,2,4-trichlorobenzene at a flow rate of 1 $cm^3\ min^{-1}$, and the analyses were performed at 140 °C. The columns were calibrated with polystyrenes having a standard narrow molar mass distribution and with linear low-density polyethylenes and polypropylenes.

The polymer melting points (Tm) and crystallinities (χ_c) were determined on a TA Instrument DSC 2920 differential scanning calorimeter connected to a thermal analyst 5000 integrator and calibrated with indium, using a heating rate of 20 °C min^{-1} in the temperature range of 30–150 °C. The heating cycle was performed twice, but only the results of the second scan are reported, because the former was influenced by the mechanical and thermal history of the samples.

SEM experiments were carried on a JEOL JSM/6060. The powder was initially fixed on a carbon tape and then coated with gold by conventional sputtering techniques.

Powder X-ray diffraction analysis was accomplished in a DIFFRAKTOMETER model D5000 (Siemens) using a Ni filter and Cu Kα (λ = 1.54 Å) radiation.

3. Results and discussion

Microporous silicates and mesoporous materials, such as alumino-silicates, alumina, chrysotile and silica–zirconia, have hydroxyl groups that may act as anchoring sites. Metallocenes can be immobilized on the surface of such materials, which involves a grafting reaction between the hydrogen (Brönsted acid sites) of the hydroxyl groups with chloride ligands from the organometallic complex. Table 1 shows the resulting grafted metal content (determined by RBS), specific surface area, pore diameter (calculated from the BET method) and catalyst activity in ethylene polymerization for the different supported systems.

As shown in Table 1, the metal content was between 0.2 and 1.0 wt.% Zr/SiO_2 or Zr/Al_2O_3. In the literature, grafted metal contents of about 0.5 and 1.0 wt.% have been reported for metallocenes on alumino-silicate and alumina supports [32]. Leaching tests with similar supported systems were shown that the amount of leached zirconocene is negligible [22].

The specific surface areas of the resulting supported metallocene catalysts were determined by nitrogen adsorption (Table 1). Textural properties of the parent supports are reported elsewhere [22]. Very low specific areas were observed for the supports prepared by the non-hydrolytic route or with natural chrysotile. Relatively high surface areas (313–478 $m^2\ g^{-1}$) were observed for the three alumino-silicates (S15, IT2 and M22). Taking into account the specific surface area and relating it to the grafted metal content, one can calculate the Zr density expressed in terms of Zr atom per square nanometer. The resulting values were from 0.06 to 1.5 Zr nm^{-2}. According to Ogasawara [33], the silanol density for silica heated at 450 °C is about 1.5 OH nm^2. Except in the cases of NHI and nCR, which were supports with very low surface areas and therefore provided supported catalysts bearing high Zr densities, most of the resulting supported metallocenes had density values much lower than those estimated for silica supports, suggesting that residual silanol groups might have been present in these materials.

The supported catalysts were further characterized by EXAFS in order to determine the interatomic distances of the constituents of these supported catalysts. Fig. 1 shows the Fourier transform of the measured signals. For NHI, SMAO, ALU and nCR, the peaks were centered at about 1.5 Å, while they were centered at about 1.3 Å for S15, IT2 and M22. All of the signals were extended up to 2 Å.

From the spectra shown in Fig. 1, during the data fitting, the low signal-to-noise relationship did not allow us to fit the structural parameters beyond the first neighbors, i.e., Zr–C and Zr–O. All of the other peaks shown after the first one were greatly affected by noise and therefore could not be assumed that correspond to real interatomic distances. Also during the data fitting, low repro-

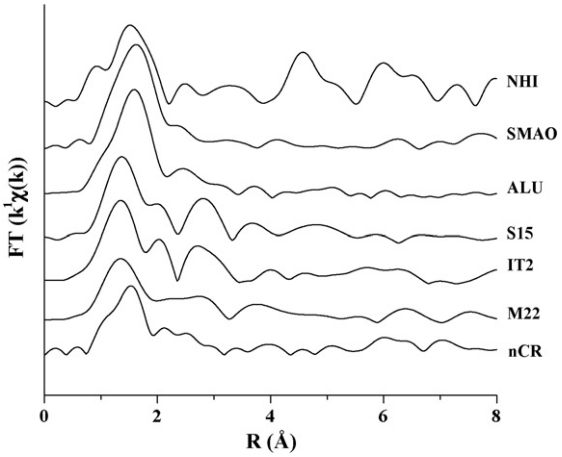

Fig. 1. Fourier Transform of EXAFS signals from the supported metallocenes.

Table 2
EXAFS parameters obtained through the first FT peak fit.

Catalysts	Bond	Distance R (Å)	χ^2
NHI	Zr–C	2.20 ± 0.02	1.2
	Zr–O	2.05 ± 0.02	
nCR	Zr–C	2.21 ± 0.02	1.9
	Zr–O	2.23 ± 0.02	
SMAO	Zr–C	2.01 ± 0.02	1.1
	Zr–O	2.17 ± 0.02	
ALU	Zr–C	2.09 ± 0.02	0.9
	Zr–O	2.19 ± 0.02	
S15	Zr–C	2.03 ± 0.02	1.5
	Zr–O	2.14 ± 0.02	
IT2	Zr–C	2.09 ± 0.02	1.4
	Zr–O	2.02 ± 0.02	
M22	Zr–C	2.05 ± 0.02	1.9
	Zr–O	2.14 ± 0.02	
Cp_2ZrCl_2	Zr–C	2.34 ± 0.02	0.5
$(n\text{BuCp})_2ZrCl_2$	Zr–C	2.35 ± 0.02	0.4

R is the interatomic distance and χ^2 is the fit quality. E_0 = Zr–C: −7.5 eV; Zr–O: −3.5 eV.

ducibility in the number of neighbors (N) and sigma values was observed, and therefore, these parameters were not explored in the present study. Thus, the structures were analyzed according to the interatomic distances (R) shown in Table 2. For comparative reasons, data from the homogeneous complexes were also included.

The results shown in Table 2 indicated that the average Zr–C distances varied between 2.01 and 2.21 Å. Such values were lower than those exhibited by the bare complexes, suggesting that the grafting reaction caused a reduction in the Zr–C interatomic distance. In the case of silica-based supports, a correlation between Zr–C interatomic distance and support pore diameter could be extracted from the data [21]. In the case of the present supports, such correlation could not be observed.

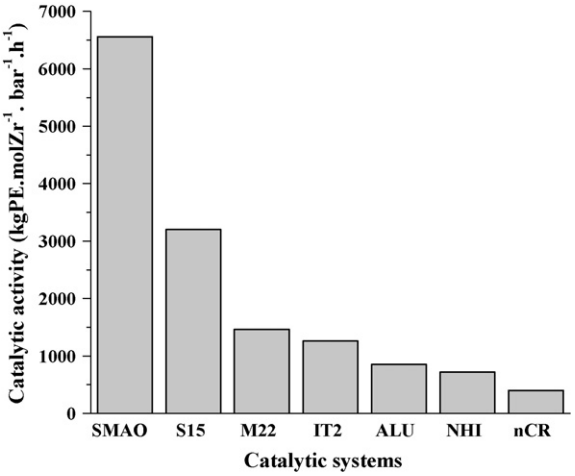

Fig. 2. Catalyst activity of the supported metallocenes in ethylene polymerization.

3.1. Catalytic activity in ethylene polymerization

The catalyst activity of the supported catalysts in ethylene polymerization is shown in Fig. 2.

Among the evaluated systems, commercial MAO-modified silica (SMAO) was shown to be the support with the highest catalyst activity, which was twice that observed in the case of S15. These supports differed in terms of textural (surface area, pore diameter, etc.), morphological (grains, fibers) and chemical (Lewis acid sites) characteristics. Thus, such results suggest that the nature of the support influences the nature of the catalyst site and the activity in ethylene polymerization.

Furthermore, textural properties also might affect catalyst activity. The presence of surface obstacles generated by the presence of micropores may cause a decrease in the catalyst activity due to problems from MAO or monomer diffusion to the catalyst center immobilized within or on the entrance of pores of small diameter [34,35]. In the supported systems presented herein, the effect

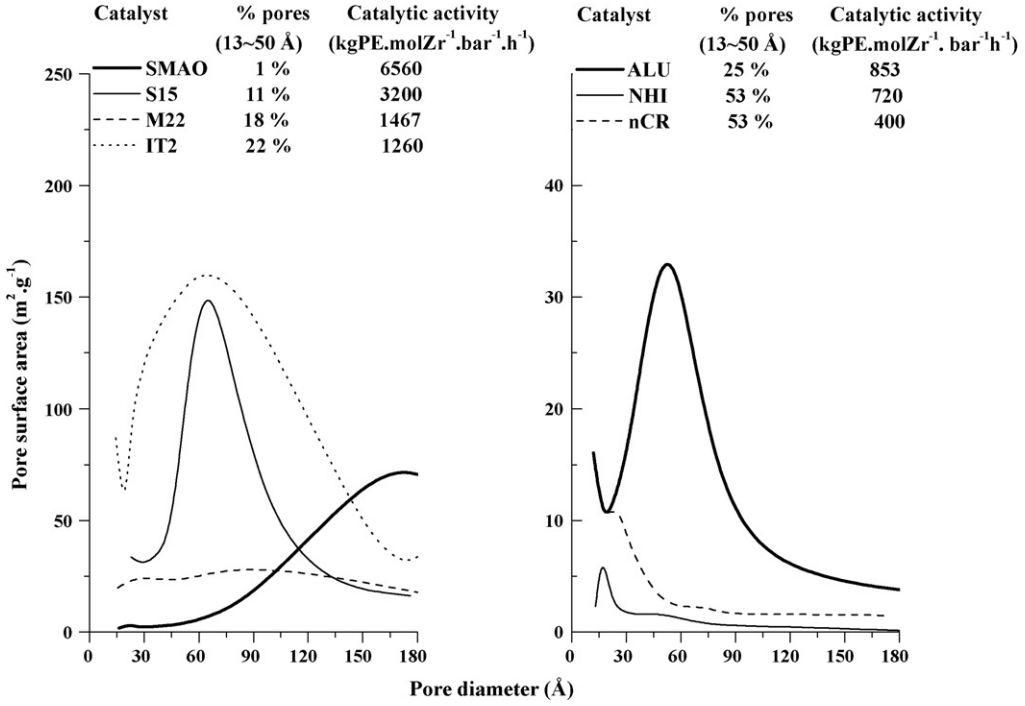

Fig. 3. Distribution curves of mean pore size as a function of pore surface area.

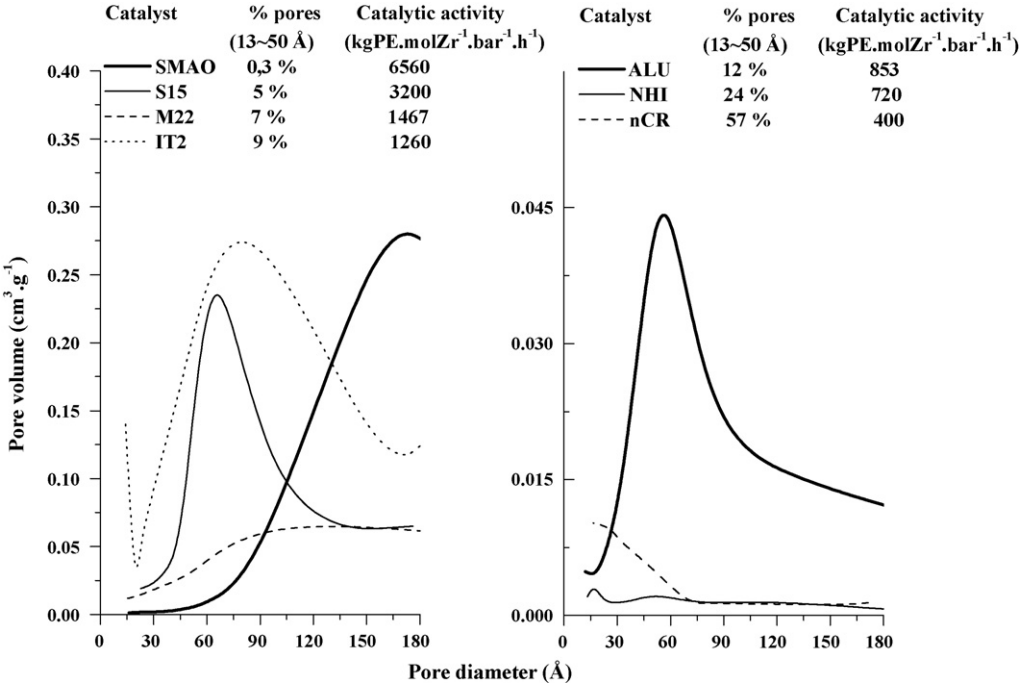

Fig. 4. Distribution curves of mean pore size as a function of pore surface volume.

of the percentage of micropores on the catalyst activity was both evaluated in terms of the pore surface area (Fig. 3) and pore volume (Fig. 4).

All of the pore size distribution curves (Figs. 3 and 4) showed two regions: one with a lower pore diameter distribution between 10 and 50 Å (here labeled as microporous), and another region, from 50 or from 80 Å, which has a larger pore diameter distribution. These curves were integrated between 13 and 50 Å and from 51 to 180 Å in order to calculate the percentage of the micropores in proportion to the total area.

The increase in the amount of the micropores caused a reduction in catalyst activity; the catalysts bearing the smallest fraction of micropores (SMAO, S15, M22 and IT2) exhibited the best activities. For the ALU, NHI and nCR systems, the catalyst activity was clearly reduced as the fraction of micropores increased. It is worth mentioning that, contrarily of that observed in the case of silica-based supports [21], no clear trend between support pore diameter and catalyst activity could be observed, as in the case of IT2 and M22, which have the smallest pore diameter. Such supported systems have micropores in a smaller proportion in comparison to other low activity supported catalysts, bearing larger pores, as in the case of ALU, NHI and nCr.

The presence of these obstacles caused by the presence of the micropores was further evaluated by the surface roughness. Atomic force microscopy (AFM) allowed for the determination of the root mean square (RMS) roughness of the surface of the catalyst particles, as shown in Fig. 5. It is worth noting that such measurement is referred to the external surface of the support particles, and not to the support surface inside the pores (in which part of the zirconocene are interacting with the support).

The relationship between the catalyst activity and surface roughness is in agreement with the trend observed in the evaluation of percentage of micropores: a large number of micropore, which affords an increase in surface roughness impinges a reduc-

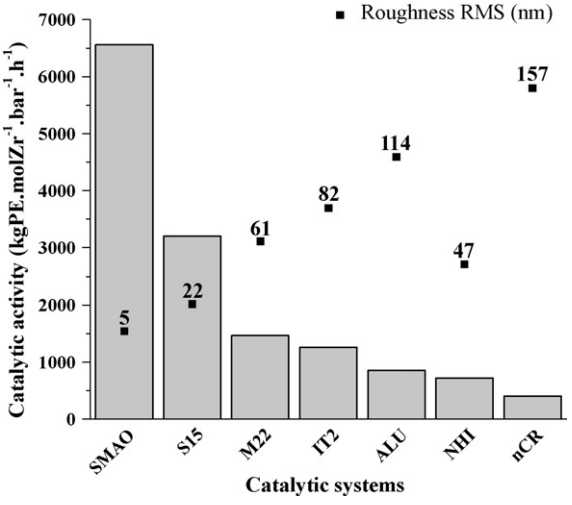

Fig. 5. RMS roughness of the metallocene-supported catalyst surface determined by AFM.

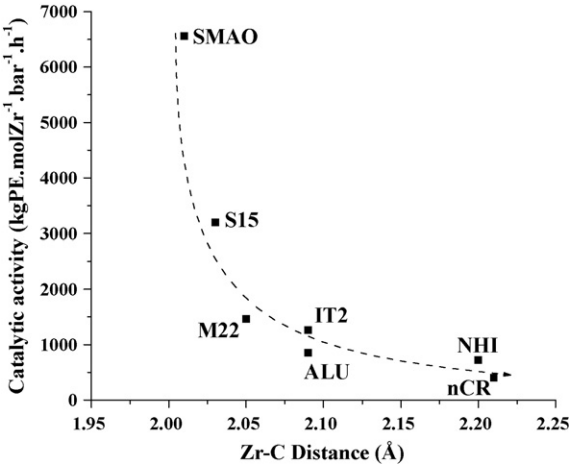

Fig. 6. Effect of interatomic Zr–C distance on the catalyst activity of the supported metallocenes.

tion in catalyst activity. Among the evaluated systems shown in Fig. 5, only NHI disagrees from this trend, probably due to drastic reduction in surface area (from 193 to 18 $m^2\ g^{-1}$ after grafting), which could be characterized by a smoother surface with fewer obstacles.

Fig. 6 shows the correlation between the interatomic distance of Zr–C and the catalyst activity.

According to Fig. 6, the catalyst activity decreased as the Zr–C distance increased. The most active systems, SMAO, S15, M22 and IT2, had supported metallocenes with mean Zr–C distances between 2.01 and 2.09 Å. Furthermore, these systems had a lower fraction of small pore size (see Figs. 4 and 5). It is worth noting that an increase in the fraction of the small pore size led to an increase in the Zr–C distance, which may be related to the proximity of the grafted metallocene and the closeness of the pore wall in the small pores. Nevertheless, one cannot neglect that one has to be cautious with such correlations since EXAFS is an average technique.

3.2. Polymer characteristics

The resulting polymers were characterized by GPC and DSC. Table 3 shows data concerning the polymer molecular weight, polydispersity index (PDI) and crystallinity (χ_c).

According to Table 3, the polymer molecular weight was between 254 and 477 kg mol^{-1}. The PDI value remained around 2.2. The largest broadening was observed in the case of polyethylene produced by S15 (2.5).

System S15 produced polymers with a molecular weight of 273 kg mol^{-1}; similar values were found by Carrero et al. [36], who grafted $(n\text{BuCp})_2ZrCl_2$ onto SBA-15, and Turunen and Pakkanen [13] (313 kg mol^{-1}), who also immobilized Cp_2ZrCl_2 on this same support. A higher molecular weight was obtained in the case of the

Table 3
Polymer properties of the resulting polyethylenes.

Catalyst	Molecular weight (kg mol^{-1})	PDI	χ_c (%)
NHI	306	2.4	55.0
nCR	254	2.0	43.0
SMAO	388	2.2	15.0
ALU	351	2.2	47.0
S15	273	2.5	43.0
IT2	477	2.0	41.0
M22	275	2.1	35.0

[Zr] = 10^{-5} mol L^{-1}; [Al/Zr] = 1000; V = 0.15 L toluene; P = 1 bar ethylene; T = 60 °C; t = 30 min.

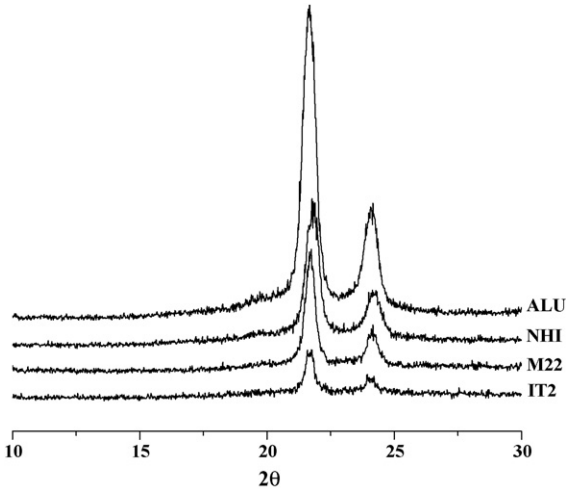

Fig. 7. XRD patterns of polyethylene obtained with ALU, NHI, M22 and IT2 supported catalysts.

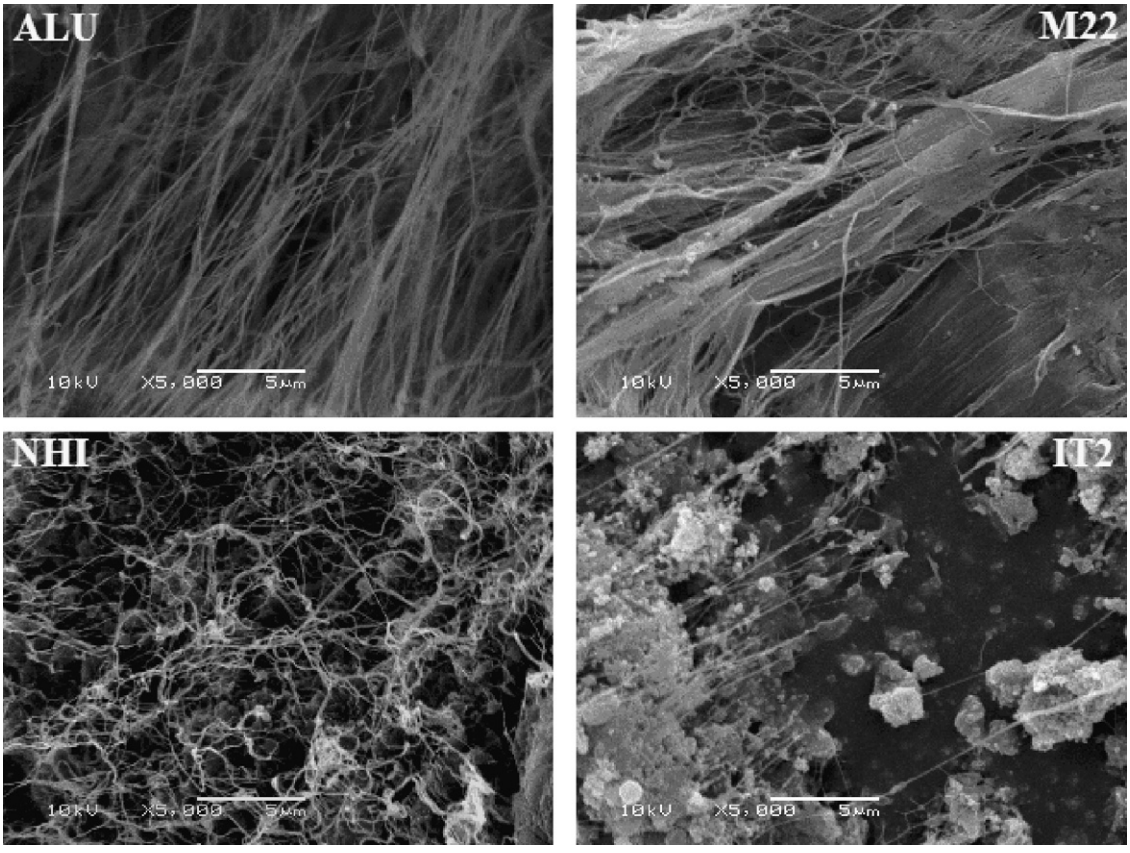

Fig. 8. SEM micrographs of polymer fibers obtained ALU, M22, NHI and IT2 with supported catalysts.

polymer produced by the ALU catalyst in comparison to those values reported by Tian et al. [37], who used Cp_2ZrMe_2, and Harrison et al. [38] with $Et(Ind)_2ZrCl_2$. In both cases, the resulting polyethylene showed a molecular weight in the range of 150 kg mol^{-1}. For MCM-22, ITQ-2 and chrysotile, no data concerning polyethylene molecular weight data was found in the literature.

According to Table 3, the polydispersity of the polymers remained in the range of 2.0–2.5, which is typical of polymers produced by single-site catalysts. The melting temperatures were roughly the same (ca. 133 °C) for all of the systems. The crystallinities varied between 15 and 55%; conversely to the phenomenon reported by Burkett et al. [39], no relationship between the crystallinity, melting temperature and support textural properties was observed in these systems.

Fig. 7 shows the XRD patterns of the polyethylene samples prepared with the ALU, NHI, M22 and IT2 supported catalysts. The orthorhombic crystalline fraction of polyethylene in the samples presented diffraction peaks at 21.7° and 24.1° for the polymers obtained with the ALU, NHI and M22 catalysts and at 21.6° and 23.9° for the polymers obtained with the IT2 catalyst, suggesting the existence of extended-chain crystals [11,12]. The small *halo* around 19.5°, particularly for the polymers obtained by ALU and NHI, indicated the existence of folded chains.

For the catalysts grafted onto alumino-silicates, the so-called polymerization through extrusion, in which the polymer chain growth takes place within the mesopores up to the particle surface, may produce polymers in fiber form [38,40,41]. The morphologies of the resultant polymers were then studied with SEM. Fig. 8 depicts the SEM micrographs of the polymers obtained with the ALU, NHI and M22 catalysts, showing the existence of polymer fibers.

The polymers obtained with the NHI, ALU and M22 catalysts presented nanofibers sized between 15.2 and 39.9 nm, calculated from the full width at the half maximum (FWHM) of the XRD peak (Fig. 7). The polymer obtained with the IT2 catalyst presented a low amount of fibers, probably due to the support delamination. The XRD analysis of this supported system showed no peaks characteristic of a lamellar structure. Only a peak centered at 24°, which was assigned to the silica *halo*, was observed, confirming the delamination process.

A correlation between the Zr–O distance (determined by EXAFS) and the polymer molecular weight (determined by GPC) was observed, as depicted by Scheme 1.

According to the literature, blocking one of the catalyst sides by grafting the metallocene on a support, affects the chain growing termination step, which causes an increase in the final molecular weight [20,42]. According to Scheme 1, as the Zr–O distance increased, the resulting polyethylene molecular weight decreased. In other words, as the metallocene becomes less sterically affected by the surface (increasing Zr–O distance), the chain termination step might be favored, thereby causing a decrease in the resulting polymer weight.

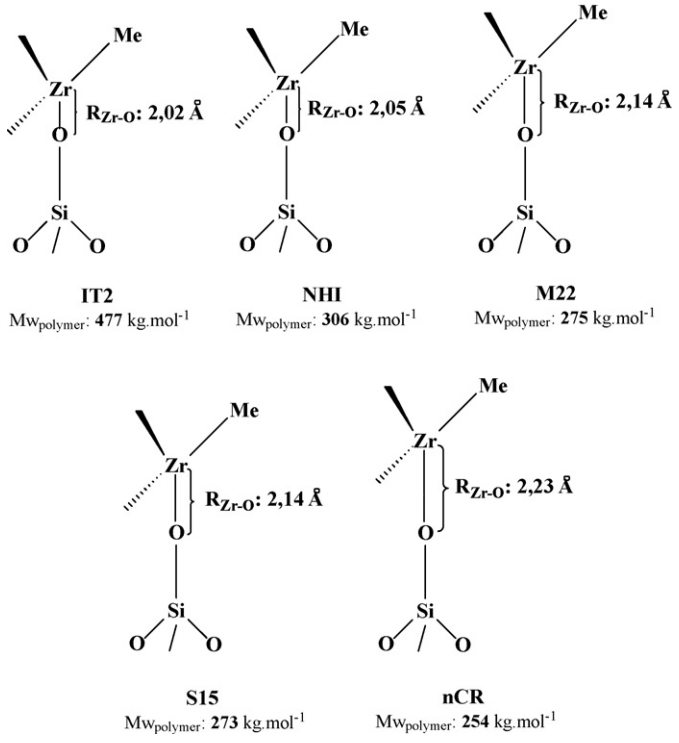

Scheme 1. Effect of the Zr–O interatomic distance on the resulting polyethylene molecular weight.

4. Conclusions

The textural characteristics of the ordered microporous and mesoporous support, such as size of porous and surface roughness, have shown influence on the structural parameters of the investigated supported systems. As previously observed by supported metallocenes grafted on mesoporous silicas, for microstructural supports the pore diameter and the pore size distribution also influenced the catalyst activity and the structure of the supported metallocenes. Supports with narrower pore diameters presented lower catalyst activities suggesting the higher probability of formation of bimolecular species due to the proximity among the catalytic precursors supported within micropores diameter smaller than approximately 50 Å. Such bimolecular species are inactive to olefin polymerization. The large fraction of pores with small diameters also contributed to the formation of surface obstacles, which might have hindered the reactant diffusion.

Furthermore, the structure of the generated metallocene surface species, which was dependent on the nature of the support, affected the Zr–O distance, which, in turn, influenced the molecular weight of the resulting polyethylene: as the Zr–O distance increased, the polyethylene molecular weight decreased.

Acknowledgements

This work was partially financed by CNPq. The authors are thankful to LNLS for measurements in the EXAFS beamline (Project D04B XAFS1#5839). Mr. William Bretas Linares from SAMA is especially thanked for providing chrysotile samples.

References

[1] G.G. Hlatky, Chem. Rev. 100 (2000) 1347–1376.
[2] J.R. Severn, J.C. Chadwick, R. Duchateau, N. Friederichs, Chem. Rev. 103 (2005) 4073–4147.
[3] S. Beck, A.R. Brough, M. Bochmann, J. Mol. Catal. A: Chem. 220 (2004) 275–284.
[4] Z. Guan, Y. Zheng, S. Jiao, J. Mol. Catal. A: Chem. 188 (2002) 123–131.
[5] M.F.V. Marques, S.C. Moreira, J. Mol. Catal. A: Chem. 192 (2003) 93–101.
[6] M. Michelotti, G. Arribas, S. Bronco, A. Altomare, J. Mol. Catal. A: Chem. 152 (2000) 167–177.
[7] C. Alonso-Moreno, D. Pérez-Quintanilla, D. Polo-Cerón, S. Prashar, I. Sierra, I. Del Hierro, M. Fajardo, J. Mol. Catal. A: Chem. 304 (2009) 107–116.
[8] J.M. Campos, J.P. Lourenço, A. Fernandes, A.M. Rego, M.R. Ribeiro, J. Mol. Catal. A: Chem. 310 (2009) 1–8.
[9] W. Kaminsky, C. Strübel, H. Lechert, D. Genske, S.I. Woo, Macromol. Rapid. Commun. 21 (2000) 909–912.
[10] C.J. Miller, D. O'Hare, Chem. Commun. 15 (2004) 1710–1711.
[11] Z.B. Ye, S.P. Zhu, W.J. Wang, H. Alsyouri, Y.S. Lin, J. Polym. Sci. Part B: Polym. Phys. 41 (2003) 2433–2443.
[12] X.C. Dong, L. Wang, W.Q. Wang, H.J. Yu, J.F. Wang, T. Chen, Z.R. Zhao, Eur. Polym. J. 41 (2005) 797–803.
[13] J.P.J. Turunen, T.T. Pakkanen, J. Mol. Catal. A: Chem. 263 (2007) 1–8.
[14] X.C. Dong, L. Wang, G.H. Jiang, Z.R. Zhao, T.X. Sun, H.J. Yu, W.Q. Wang, J. Mol. Catal. A: Chem. 240 (2005) 239–244.

[15] X.C. Dong, L. Wang, W.Q. Wang, G.H. Jiang, Y. Chen, Z.R. Zhao, J.J. Wang, Macromol. Mater. Eng. 290 (2005) 31–37.
[16] J.C. Hicks, A. Mullis, C.W. Jones, J. Am. Chem. Soc. 129 (2007) 8426–8427.
[17] S.P. Varkey, R.F. Lobo, K.H. Theopold, Catal. Lett. 88 (2003) 227–229.
[18] C. Covarrubias, R. Quijada, R. Rojas, Micropor. Mesopor. Mater. 117 (2009) 118–125.
[19] (a) M.W. McKittrici, C.W. Jones, Chem. Mater. 17 (2005) 4758–4761, See, for example;
(b) R.M. Kasi, E.B. Coughlin, Organometallics 22 (2003) 1534–1539.
[20] W. Kaminsky, F. Renner, Makromol. Chem. Rapid. Commun. 14 (1993) 239–248.
[21] F. Silveira, M.C.M. Alves, F.C. Stedile, S.B. Pergher, A. Rigacci, J.H.Z. Dos Santos, J. Mol. Catal. A: Chem. 298 (2009) 40–50.
[22] F. Silveira, C.F. Petry, D. Pozebon, S.B. Phergher, C. Detoni, F.C. Stedile, J.H.Z. Dos Santos, A. Rigacci, Appl. Catal. A: Gen. 333 (2007) 96–106.
[23] F. Silveira, G.P. Pires, C.F. Petry, D. Pozebon, F.C. Stedile, J.H.Z. Dos Santos, A. Rigacci, J. Mol. Catal. A: Chem. 265 (2007) 167–176.
[24] S.B.C. Pergher, A. Corma, V. Fornés, Quím. Nov. 26 (2003) 795–802.
[25] A. Corma, V. Fornés, S.B.C. Pergher, T.L.M. Maessen, J.G. Buglass, Nature 396 (1998) 353–356.
[26] A.G. Fisch, N.S.M. Cardozo, A.R. Secchi, F.C. Stedile, N.P. Da Silveira, J.H.Z. Dos Santos, J. Non-Cryst. Sol. 354 (2008) 3973–3979.
[27] F.C. Stedile, J.H.Z. Dos Santos, Phys. Stat. Sol. 173 (1999) 123–134.
[28] I. Horcas, R. Fernandez, J.M. Gomez-Rodriguez, J. Colchero, J. Gomez-Herrero, A.M. Baro, Ver. Sci. Instrum. 78 (2007) 1–8.
[29] T. Ressler, J. Synchrotron Radiat. 5 (1998) 118–122.
[30] J.J. Rehr, R.C. Albers, Rev. Mod. Phys. 72 (2000) 621–654.
[31] B. Ravel, J. Synchrotron Radiat. 8 (2001) 4–316.
[32] M. Jezequel, V. Dufaud, M.J. Ruiz-Garcia, F. Carrillo-Hermosilla, U. Neugebauer, G.P. Niccolai, F. Lefebvre, F. Bayard, J. Corker, S. Fiddy, J. Evans, J.P. Broyer, J. Malinge, J.M. Basset, J. Am. Chem. Soc. 123 (2001) 3520–3540.
[33] S. Ogasawara, Shokubai 18 (1976) 124–134.
[34] M.P. McDaniel, Adv. Catal. 33 (1985) 47–98.
[35] A. Stein, B.J. Melde, R.C. Schroden, Adv. Mater. 12 (2000) 1403–1419.
[36] A. Carrero, R. Van Grieken, I. Suarez, B. Paredes, Polym. Eng. Sci. 48 (2008) 606–616.
[37] J. Tian, S. Wang, Y. Feng, J. Li, S. Collins, J. Mol. Catal. A: Chem. 144 (1999) 137–150.
[38] D. Harrison, I.M. Couter, S. Wang, S. Nistala, B.A. Kuntz, M. Pingeon, J. Tian, S. Collins, J. Mol. Catal. A: Chem. 128 (1998) 65–77.
[39] S.L. Burkett, S. Soukasene, K.L. Milton, R. Welch, A.J. Little, R.M. Kasi, E.B. Coughlin, Chem. Mater. 17 (2005) 2716–2723.
[40] D.T. On, D. Desplantier-Giscard, C. Danumah, S. Kaliaguine, Appl. Catal. A: Gen. 222 (2001) 299–357.
[41] C. Guo, D. Zhang, F. Wang, G.-X. Jin, J. Catal. 234 (2005) 356–363.
[42] J.H.Z. Dos Santos, C. Krug, M.B. Da Rosa, F.C. Stedile, J. Dupont, M.M.C. Forte, J. Mol. Catal. Chem. 139 (1999) 199–207.